Supporting Information

Delayed photoacidity produced through the triplet-triplet annihilation of a neutral pyranine derivative

J. Christian Lennox,[a] Evgeny O. Danilov,[b] Jillian L. Dempsey[a]*

[a]*Department of Chemistry, University of North Carolina, Chapel Hill, North Carolina, United States*

[b]*Department of Chemistry, North Carolina State University, Raleigh, North Carolina, United States*

*Correspondence to dempseyj@email.unc.edu

Table of Contents

EXPERIMENTAL

General Considerations. Trisodium 8-Acetoxypyrene-1,3,6-trisulfonic Acid was prepared according to a literature procedure,[1] Acetonitrile (Fisher Scientific, HPLC >99.9%) was degassed with argon, dried with a Pure Process Technology Solvent System, and stored over 3 Å molecular sieves in a nitrogen-filled glovebox. Tetrabutylammonium hexafluorophosphate ($[NBu_4][PF_6]$, Oakwood Chemical, 98%) was recrystallized from absolute ethanol, dried in vacuo, and stored under inert atmosphere. All other reagents were commercially available and used without further purification.

^{1}H NMR spectra were recorded at room temperature using a 400 or 600 MHz Bruker NMR spectrometer. All deuterated solvents were purchased from Cambridge Isotope Laboratories and used without further purification.

All samples used for spectroscopic studies were prepared with rigorously dried acetonitrile in a nitrogen-filled glovebox. Photoacid samples were prepared in 0.1 M $[NBu_4][PF_6]$ acetonitrile solution and concentrations typically ranged between 20-60 μM. Samples were placed into 1 cm path length quartz cuvettes and isolated from atmosphere with a Teflon Kontes valve.

Optical Characterization. UV-vis absorbance measurements were recorded using a Cary 60 UV-vis absorbance spectrometer using a 1 cm path length quartz cuvette. Steady-state photoluminescence spectra were obtained using an Ocean Optics USB2000+ spectrometer with excitation via a 365 nm laser diode. Emission intensities at each wavelength were corrected for nonlinear spectrometer response. Time-correlated simple photon counting (TCSPC) measurements were recorded using an Edinburgh Instruments FLS920 equipped with a 444.2 nm diode laser (Edinburgh Instruments EPL-445, 73 ps FWHM pulse width) operated at 10 MHz. Time-gated photoluminescence spectra were obtained using an Edinburgh Instruments LP920 laser flash photolysis system equipped with an ICCD detector.

Transient Absorption Spectroscopy. Transient absorption experiments were performed using a custom-build laser flash photolysis system. Laser excitation (5-7 ns FWHM, 10 Hz, Q-switched) was provided by the third harmonic of a Nd:YAG laser (Spectra-Physics, Inc., model Quanta-Ray LAB-170-10) that pumped an OPO (basiScan, GWU Lasertechnik) to access tunable excitation (415–800 nm). Laser power at the sample cuvette was attenuated by the use of a half-wave plate (WPMH10M-355, ThorLabs) and polarizer (GL10-A, ThorLabs). A glass window was used to deflect a small portion of excitation beam to a Si diode detector (DET10A, ThorLabs), triggering the oscilloscope to start data collection. Timing of the laser was controlled by a digital delay generator (9514+ Pulse Generator, Quantum Composers). A 75 watt Xe Arc Lamp (PowerArc, Optical Building Blocks) was used in continuous wave mode as a white light source. The probe beam was passed through a 375 nm long pass filter before passing through the sample collinear with the pump beam. Probe light was then attenuated using a neutral density filter, and scattered excitation light filtered with a color filter wheel containing various long pass and short pass filters. Single wavelength kinetics were obtained using a double slit monochromator (Spectral Products CM112) outfitted with a Hamamatsu R928 photomultiplier tube (PMT). The signal was amplified by a 200 MHz wideband voltage amplifier (DHPVA-200, Electro Optical Components), and processed using a digitizer (CompuScope 12502, GaGeScope) controlled by custom software (MATLAB). The data were converted to units of ΔOD (ΔOD = -log(I/I_0), where I is the time-resolved probe light intensity with laser excitation, and I_0 is the intensity without excitation). Data were collected at room temperature and further analyzed in Igor Pro 6.22 (Wavemetrics).

Synthesis of N^1,N^1,N^3,N^3,N^6,N^6-hexaethyl-8-hydroxypyrene-1,3,6-trisulfonamide (^{Et}HPTA-OH). 1.04 g (1.84 mmol) of trisodium 8-acetoxypyrene-1,3,6-trisulfonic acid was suspended in a mixture of thionyl chloride (5 mL) and five drops of dimethyl formamide. The reaction was heated to reflux under nitrogen for 5 hours. The color evolved from gray to yellow to orange throughout the reaction. After cooling to

room temperature, excess thionyl chloride was removed via nitrogen stream and bubbled through a scrubbing solution of saturated aqueous sodium carbonate. The flask was cooled to 0 °C and a solution of 5 mL of diethylamine in 10 mL of dichloromethane was added dropwise, causing the evolution of gray smoke. The solution was warmed to room temperature and stirred for 24 hours. 1 M HCl was added slowly to deacetylate and to quench unreacted sulfonyl chloride moieties. Dichloromethane and excess diethylamine were removed via rotary evaporator, and the remaining aqueous solution was filtered to remove a yellow precipitate. The precipitate was purified via column chromatography (eluent 60:40 ethyl acetate:pentane, silica stationary phase) to obtain a yellow powder (337 mg, 29.4%). ^{1}H NMR (600 MHz, $CDCl_3$) δ 9.21 (s, 1H), 9.17 (d, J = 9.7 Hz, 1H), 9.14 (d, J = 9.6 Hz, 1H), 9.01 (d, J = 9.8 Hz, 1H), 8.80 (d, J = 9.6 Hz, 1H), 8.37 (s, 1H), 3.47 – 3.52 (m, 12H), 1.22 – 1.15 (m, 18H). ^{13}C{^{1}H} NMR (151 MHz, $CDCl_3$) δ 152.81, 135.61, 132.24, 132.11, 132.05, 131.19, 128.42, 127.66, 126.54, 126.18, 125.67, 124.44, 122.59, 121.52, 120.75, 116.40, 41.45, 41.43, 41.06, 13.88, 13.86, 13.57. ESI-MS *m/z* 622.17228, calcd for ^{Et}HPTA-O$^-$ ($C_{28}H_{36}N_3O_7S_3^-$): 622.17. Anal. Calcd.: C, 53.91; H, 5.98; N, 6.74; S, 15.42. Found: C, 53.32; H, 5.93; N, 6.73; S, 15.22.

Synthesis of 1-Methyl-[4,4'-bipyridin]-1-ium Hexafluorophosphate ([MQ]PF_6).

Following a modified literature procedure,[2] 4,4'-bipyridine (3.61 g, 22.0 mmol) and iodomethane (1.60 mL, 28.0 mmol) were combined in 20 mL dichloromethane and heated to reflux for 1 h. A yellow solid was filtered off and washed with ethyl acetate. The solid (crude 1-methyl-[4,4'-bipyridin]-1-ium iodide) was dissolved in 20 mL of 1:1 methanol:water along with an excess of potassium hexafluorophosphate. The solution was heated to ca. 50 °C for 30 minutes, then cooled to room temperature. After sitting for 30 minutes, the solution was filtered to isolate a white precipitate, which was subsequently redissolved in acetonitrile and recrystallized via vapor diffusion of diethyl ether to yield pure [MQ](PF_6).

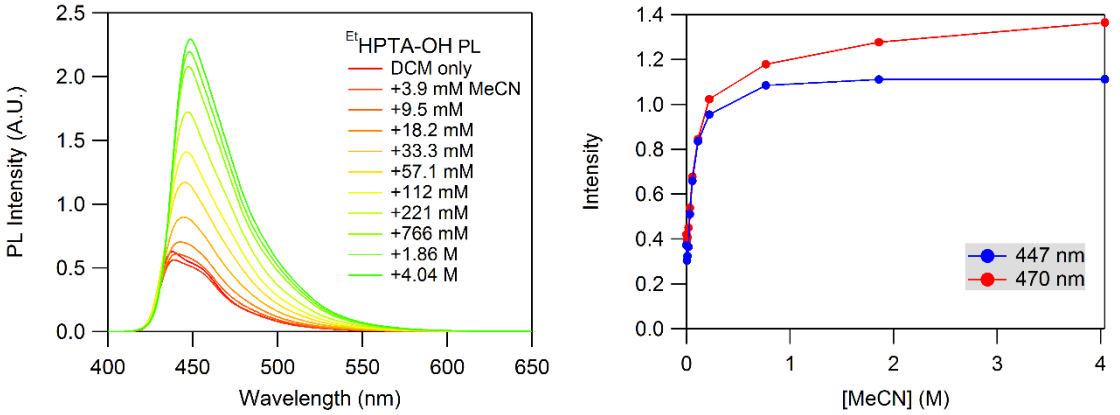

Figure S1: (Left) Photoluminescence spectra throughout a titration of acetonitrile into a solution of ^{Et}HPTA-OH in dichloromethane, and (Right) Peak heights from Gaussian deconvolution of the emission bands at 447 nm and 470 nm that correspond to the ^1L_b and ^1L_a states respectively. Upon the addition of a more polar, hydrogen-bonding solvent (acetonitrile), increases in the emission from both bands are observed. Greater enhancement is seen of emission from the band at 470 nm, supporting the assignment of this band as emission from the ^1L_a state.[3,4] Spectra are corrected for dilution. λ_{exc} = 365 nm.

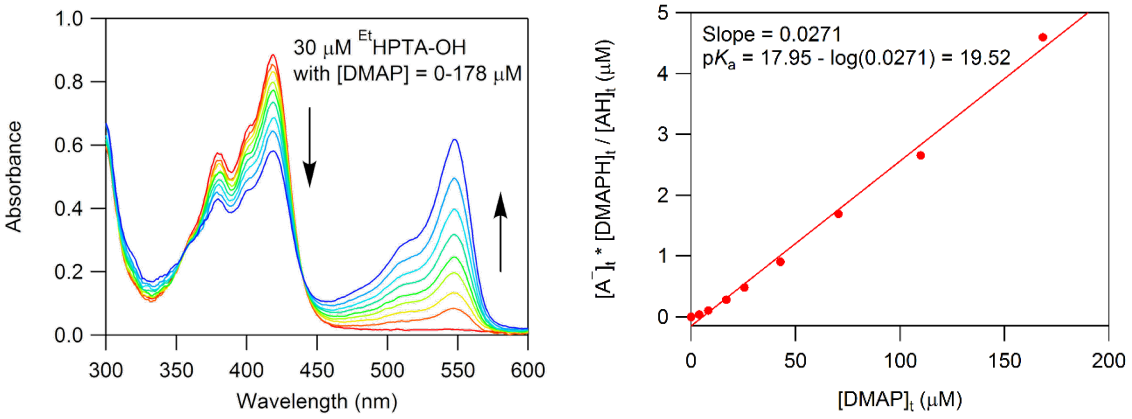

Figure S2. (Left) Spectrophotometric titration of ^{Et}HPTA-OH with N,N-dimethylpyridin-4-amine (DMAP) (pK_a = 17.95) in acetonitrile, and (right) plot of titrant and analyte concentrations used to obtain the pK_a of ^{Et}HPTA-OH (19.52).

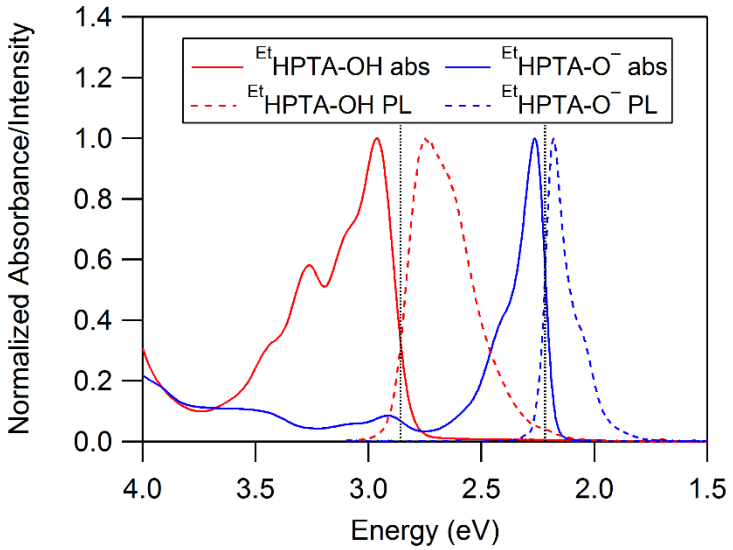

Figure S3. The intercept of the normalized absorption and emission spectra for ^{Et}HPTA-OH and ^{Et}HPTA-O$^-$ yield E_{00} values of 2.86 eV and 2.22 eV respectively.

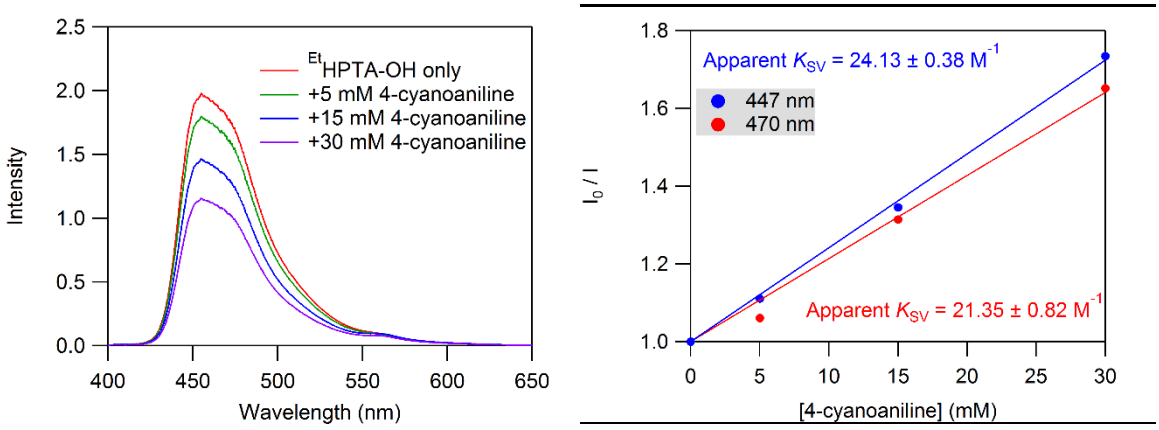

Figure S4: Steady-state fluorescence spectra and Stern-Volmer fit of ^{Et}HPTA-OH with varying concentrations of 4-cyanoaniline. Intensity measurements are obtained via peak heights of Gaussian deconvolution of the ^1L_b and ^1L_a emission bands at 447 nm and 470 nm respectively. Spectra are corrected for dilution. λ_{exc} = 365 nm.

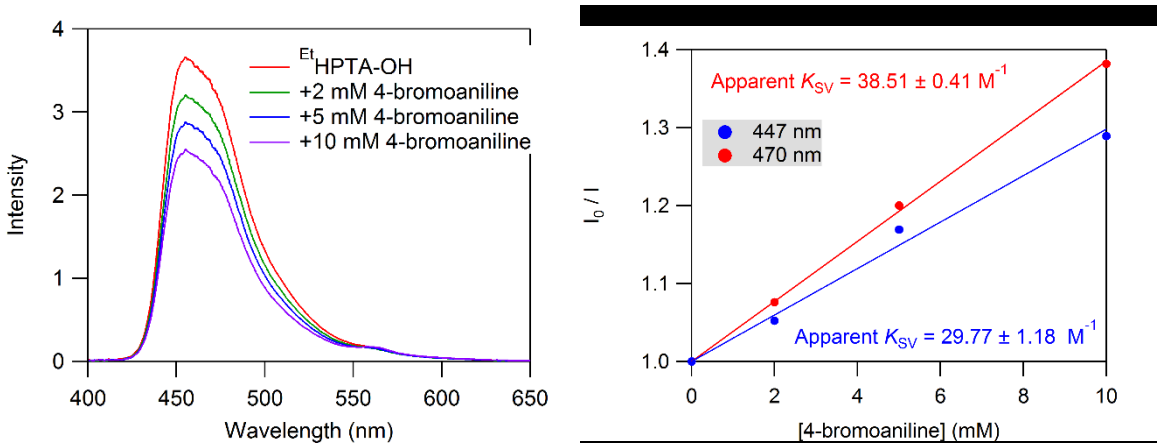

Figure S5: Steady-state fluorescence spectra and Stern-Volmer fit of ^{Et}HPTA-OH with varying concentrations of 4-bromoaniline. Intensity measurements are obtained via peak heights of Gaussian deconvolution of the ^1L_b and ^1L_a emission bands at 447 nm and 470 nm respectively. Spectra are corrected for dilution. λ_{exc} = 365 nm.

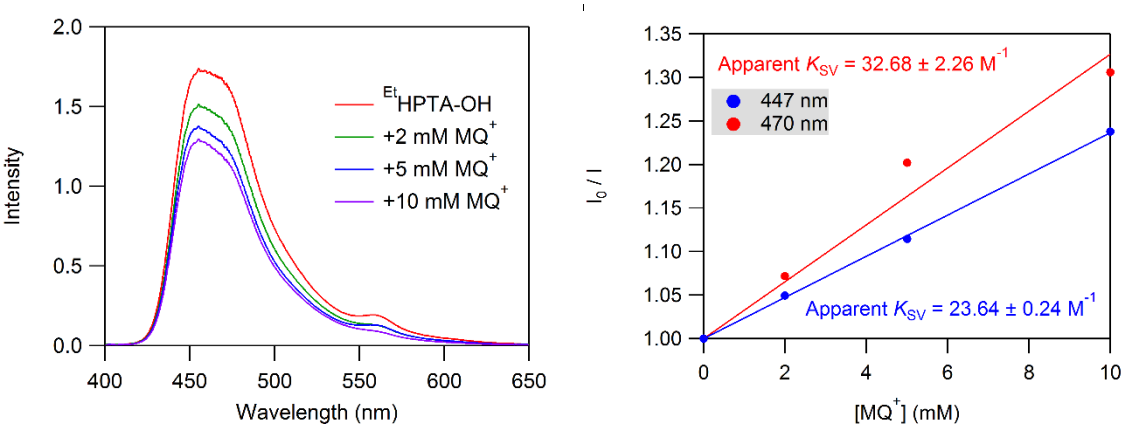

Figure S6: Steady-state fluorescence spectra and Stern-Volmer fit of ^{Et}HPTA-OH with varying concentrations of MQ^+. Intensity measurements are obtained via peak heights of Gaussian deconvolution of the ^1L_b and ^1L_a emission bands at 447 nm and 470 nm respectively. Spectra are corrected for dilution. λ_{exc} = 365 nm.

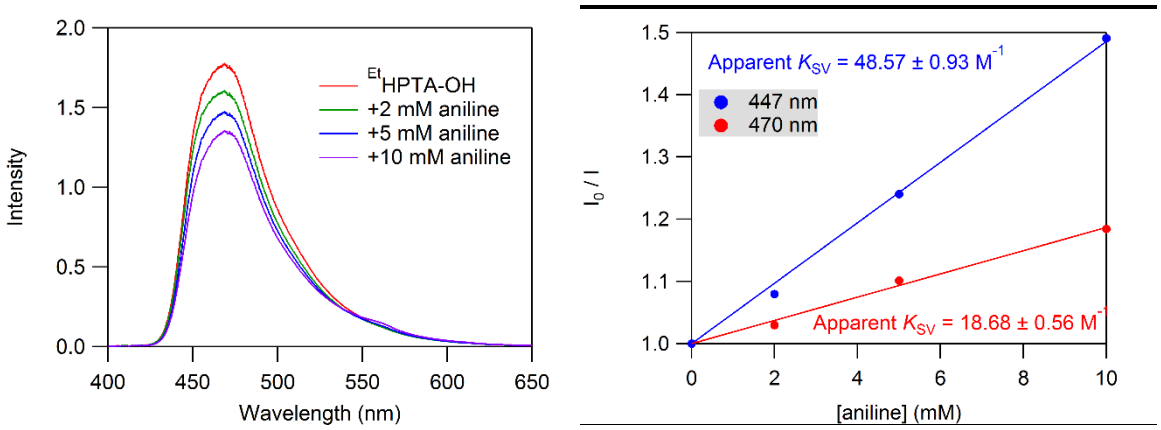

Figure S7: Steady-state fluorescence spectra and Stern-Volmer fit of ^{Et}HPTA-OH with varying concentrations of aniline. Intensity measurements are obtained via peak heights of Gaussian deconvolution of the ^1L_b and ^1L_a emission bands at 447 nm and 470 nm respectively. Spectra are corrected for dilution. λ_{exc} = 365 nm.

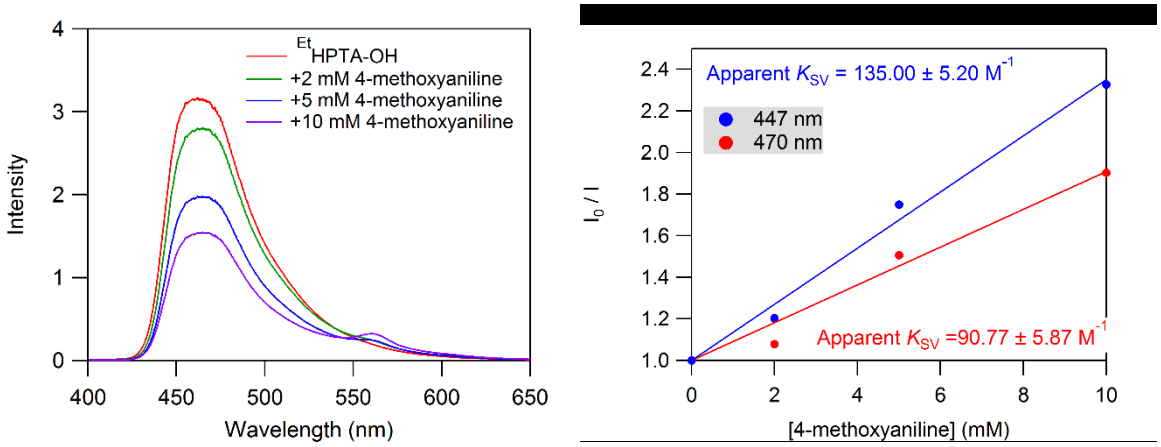

Figure S8: Steady-state fluorescence spectra and Stern-Volmer fit of ^{Et}HPTA-OH with varying concentrations of 4-methoxyaniline. Intensity measurements are obtained via peak heights of Gaussian deconvolution of the ^1L_b and ^1L_a emission bands at 447 nm and 470 nm respectively. Spectra are corrected for dilution. λ_{exc} = 365 nm.

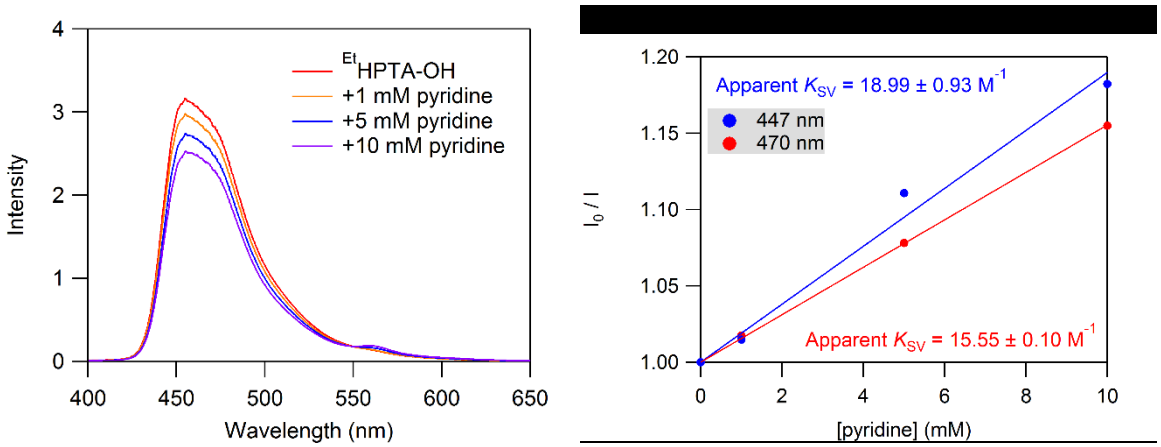

Figure S9: Steady-state fluorescence spectra and Stern-Volmer fit of ^{Et}HPTA-OH with varying concentrations of pyridine. Intensity measurements are obtained via peak heights of Gaussian deconvolution of the ^1L_b and ^1L_a emission bands at 447 nm and 470 nm respectively. Spectra are corrected for dilution. λ_{exc} = 365 nm.

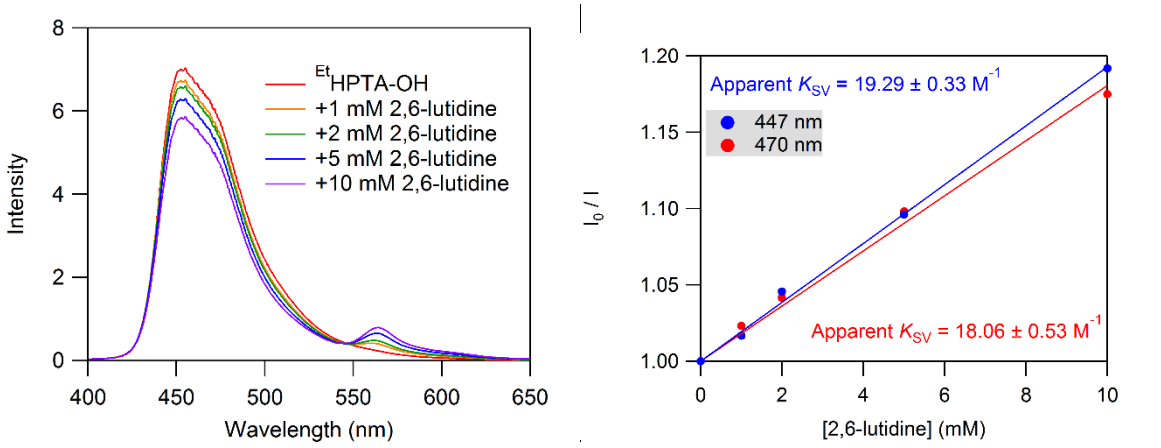

Figure S10: Steady-state fluorescence spectra and Stern-Volmer fit of ^{Et}HPTA-OH with varying concentrations of 2,6-lutidine. Intensity measurements are obtained via peak heights of Gaussian deconvolution of the ^1L_b and ^1L_a emission bands at 447 nm and 470 nm respectively. Spectra are corrected for dilution. λ_{exc} = 365 nm.

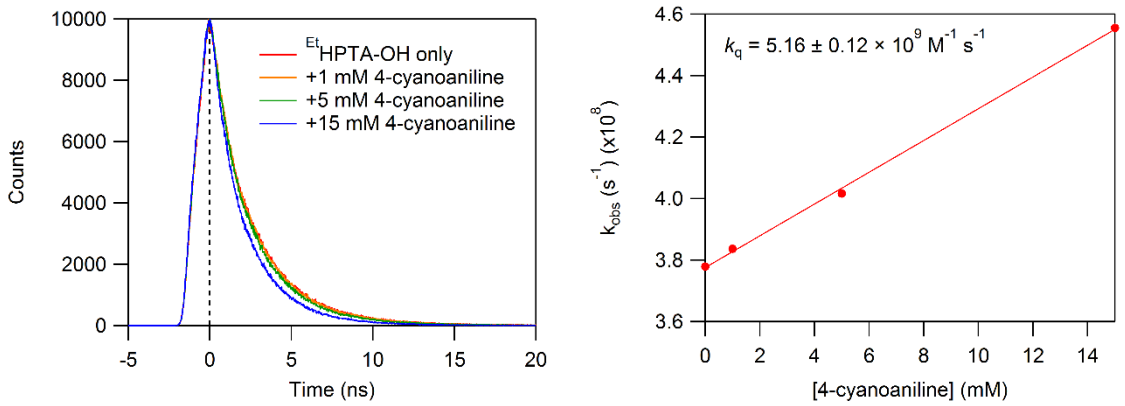

Figure S11. (Left) TCSPC time-resolved fluorescence traces of ^{Et}HPTA-OH in presence of 0-15 mM 4-cyanoaniline and (right) Stern-Volmer plot of fluorescence quenching yields k_q = 5.16 ± 0.12 × 10^9 M^{-1} s^{-1}. λ_{exc} = 444.2 nm, λ_{em} = 480 nm. In acetonitrile with 0.1 M [NBu_4][PF_6]

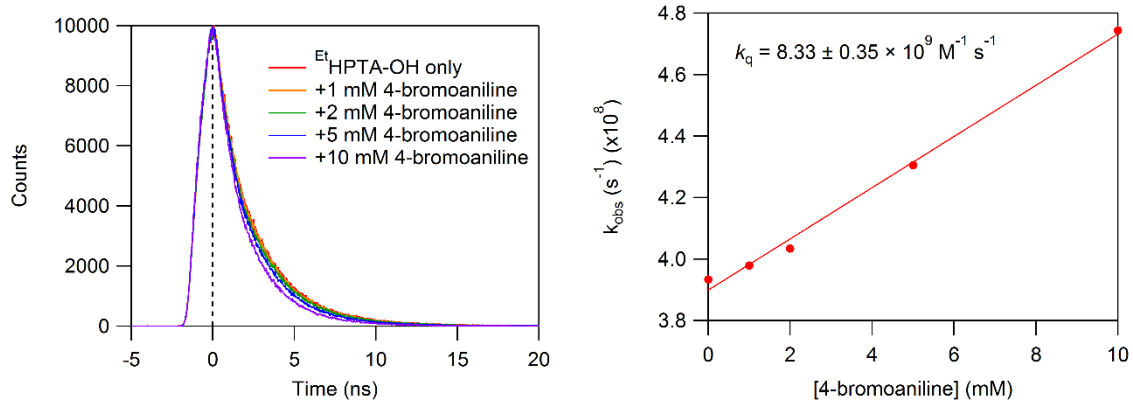

Figure S12. (Left) TCSPC time-resolved fluorescence traces of ^{Et}HPTA-OH in presence of 0-10 mM 4-bromoaniline and (right) Stern-Volmer plot of fluorescence quenching yields k_q = 8.33 ± 0.35 × 10^9 M^{-1} s^{-1}. λ_{exc} = 444.2 nm, λ_{em} = 480 nm. In acetonitrile with 0.1 M [NBu_4][PF_6]

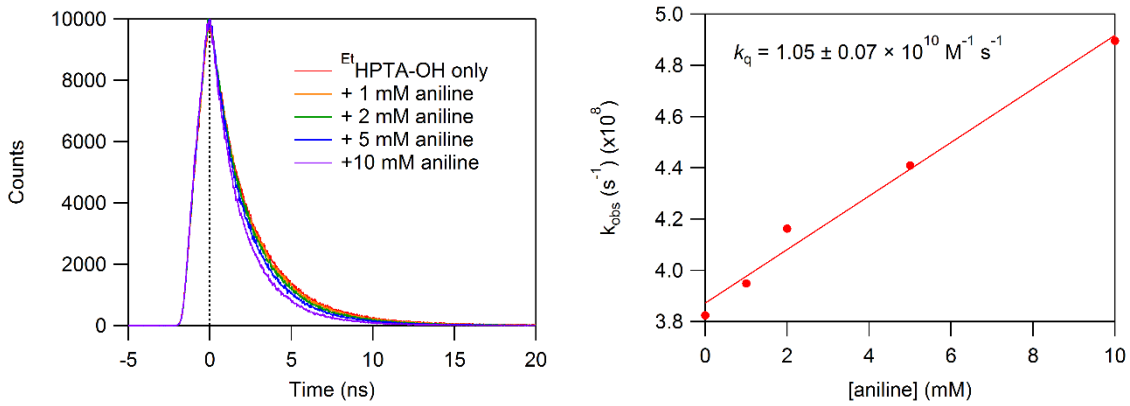

Figure S13. (Left) TCSPC time-resolved fluorescence traces of ^{Et}HPTA-OH in presence of 0-10 mM aniline and (right) Stern-Volmer plot of fluorescence quenching yields k_q = 1.05 ± 0.07 × 10^{10} M^{-1} s^{-1}. λ_{exc} = 444.2 nm, λ_{em} = 480 nm. In acetonitrile with 0.1 M [NBu_4][PF_6].

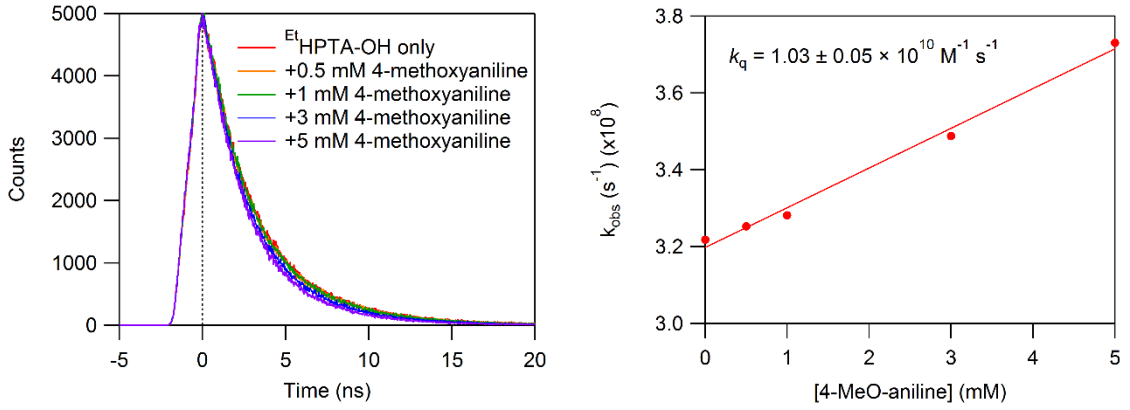

Figure S14. (Left) TCSPC time-resolved fluorescence traces of ^{Et}HPTA-OH in presence of 0-5 mM 4-methoxyaniline and (right) Stern-Volmer plot of fluorescence quenching yields k_q = 1.03 ± 0.05 × 10^{10} M^{-1} s^{-1}. λ_{exc} = 444.2 nm, λ_{em} = 480 nm. In acetonitrile with 0.1 M [NBu_4][PF_6]

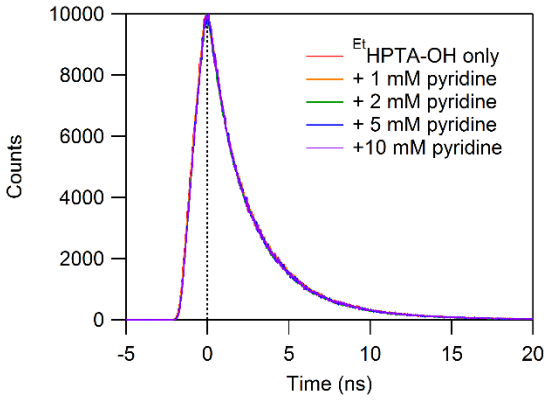

Figure S15. TCSPC time-resolved fluorescence traces of ^{Et}HPTA-OH in presence of 0-10 mM pyridine. No dynamic quenching was observed. λ_{exc} = 444.2 nm, λ_{em} = 480 nm. In acetonitrile with 0.1 M [NBu_4][PF_6]

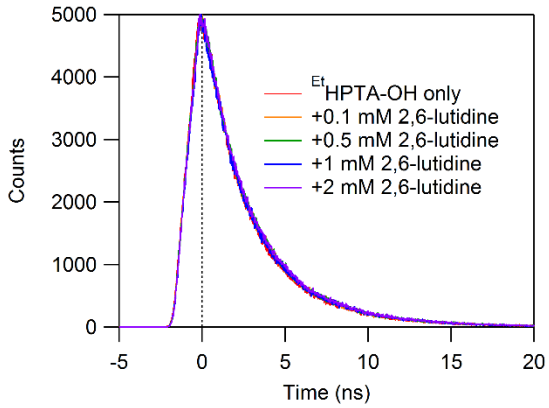

Figure S16. TCSPC time-resolved fluorescence traces of ^{Et}HPTA-OH in presence of 0-2 mM 2,6-lutidine. No dynamic quenching was observed. λ_{exc} = 444.2 nm, λ_{em} = 480 nm. In acetonitrile with 0.1 M [NBu_4][PF_6]

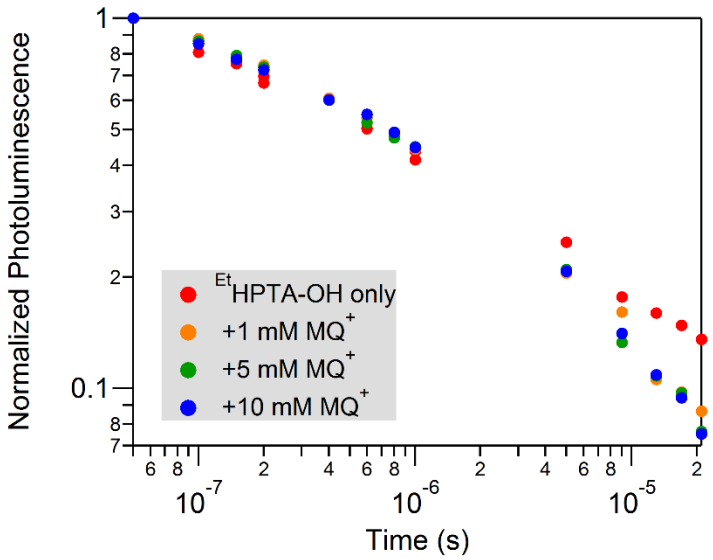

Figure S17. Normalized counts of delayed fluorescence from ^{Et}HPTA-OH measured at 450 nm. Increasing concentrations of MQ^+ do not lead to a reduction in ^{Et}HPTA-OH triplet lifetime.

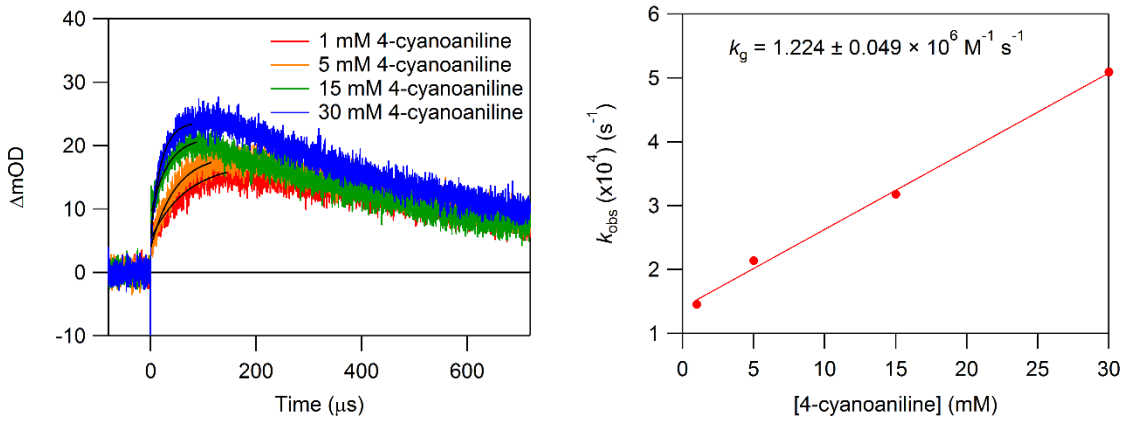

Figure S18. (Left) Growth and decay of photoproduct ^{Et}HPTA-O$^-$ as quantified via transient absorption traces at 548 nm with varying concentrations of 4-cyanoaniline and (right) plot of observed rate constants for the slow growth of the transient at 548 nm versus the concentration of 4-cyanoaniline yields the apparent second-order rate constant for growth of in acetonitrile with 0.1 M [NBu$_4$][PF$_6$].

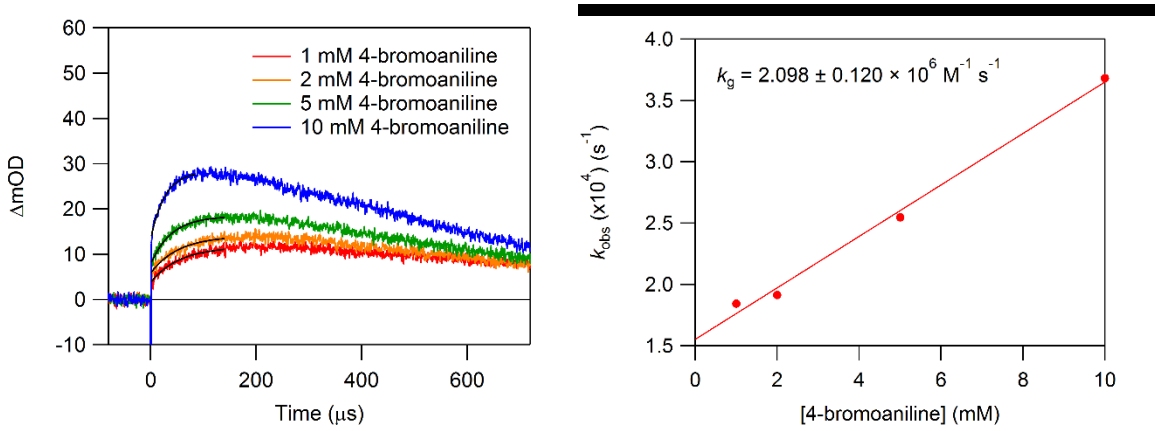

Figure S19. (Left) Growth and decay of photoproduct ^{Et}HPTA-O$^-$ as quantified via transient absorption traces at 548 nm with varying concentrations of 4-bromoaniline and (right) plot of observed rate constants for the slow growth of the transient at 548 nm versus the concentration of 4-bromoaniline yields the apparent second-order rate constant for growth of in acetonitrile with 0.1 M [NBu$_4$][PF$_6$].

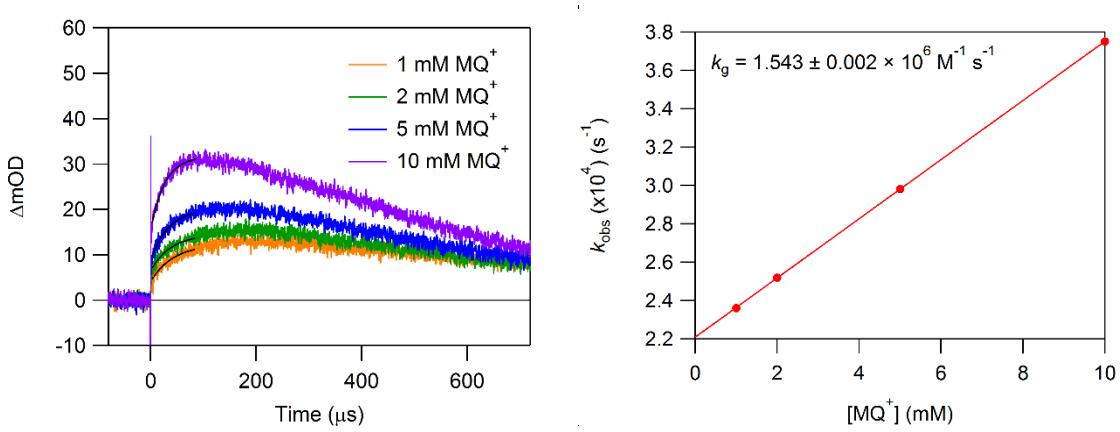

Figure S20. (Left) Growth and decay of photoproduct ^{Et}HPTA-O$^-$ as quantified via transient absorption traces at 548 nm with varying concentrations of MQ^+ and (right) plot of observed rate constants for the slow growth of the transient at 548 nm versus the concentration of MQ^+ yields the apparent second-order rate constant for growth of in acetonitrile with 0.1 M [NBu_4][PF_6].

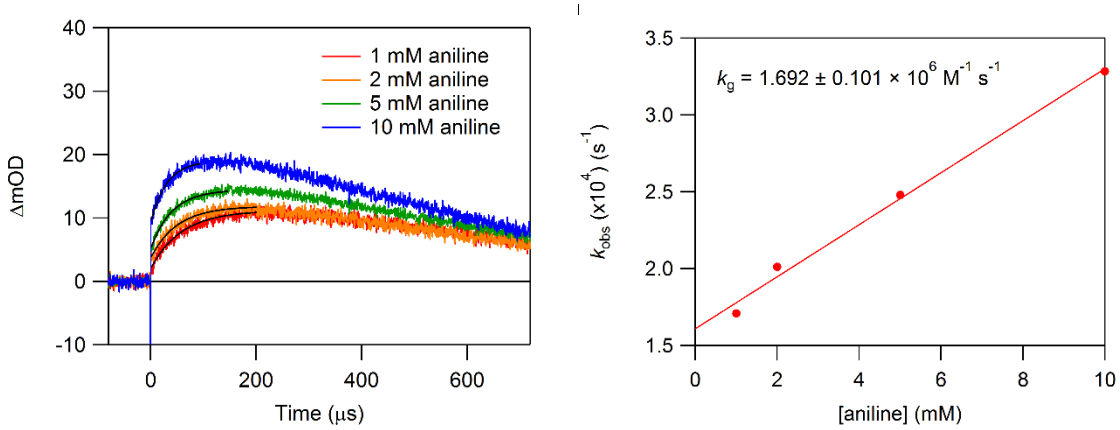

Figure S21. (Left) Growth and decay of photoproduct ^{Et}HPTA-O$^-$ as quantified via transient absorption traces at 548 nm with varying concentrations of aniline and (right) plot of observed rate constants for the slow growth of the transient at 548 nm versus the concentration of aniline yields the apparent second-order rate constant for growth of in acetonitrile with 0.1 M [NBu_4][PF_6].

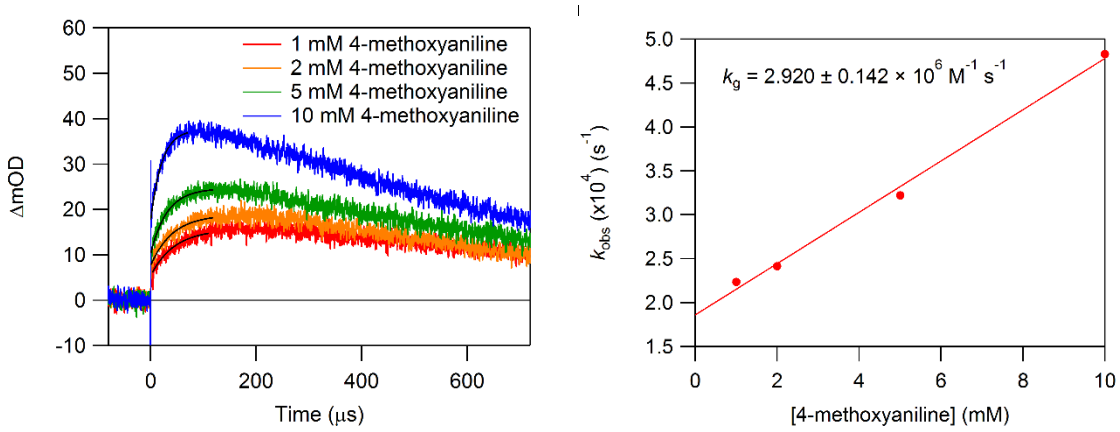

Figure S22. (Left) Growth and decay of photoproduct ^{Et}HPTA-O$^-$ as quantified via transient absorption traces at 548 nm with varying concentrations of 4-methoxyaniline and (right) plot of observed rate constants for the slow growth of the transient at 548 nm versus the concentration of 4-methoxyaniline yields the apparent second-order rate constant for growth of in acetonitrile with 0.1 M [NBu$_4$][PF$_6$].

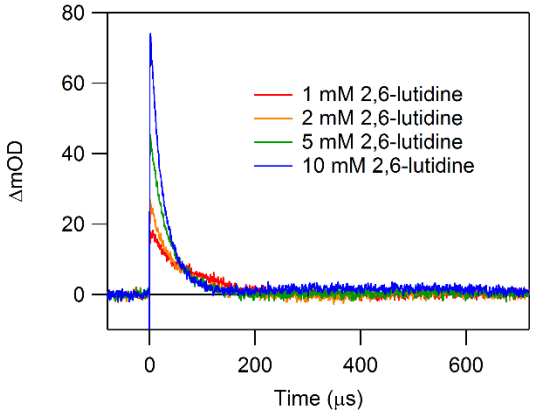

Figure S23. Decay of photoproduct ^{Et}HPTA-O$^-$ as quantified via transient absorption traces at 548 nm with varying concentrations of 2,6-lutidine in acetonitrile with 0.1 M [NBu$_4$][PF$_6$].

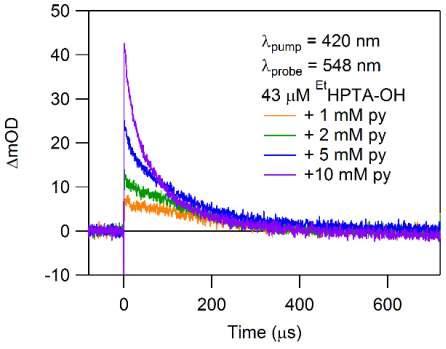

Figure S24. Decay of photoproduct ^{Et}HPTA-O$^-$ as quantified via transient absorption traces at 548 nm with varying concentrations of pyridine in acetonitrile with 0.1 M [NBu$_4$][PF$_6$].

Scheme S1. Basic kinetics model used to find k_{BPT} from the recombination of ^{Et}HPTA-O$^-$ and the conjugate acid of added base.

$$^{Et}\text{HPTA-O}^- + \text{BH}_+ \xrightarrow{k_{BPT}} {}^{Et}\text{HPTA-OH} + \text{B}$$

$$\frac{d[^{Et}\text{HPTA-O}^-]}{dt} = -k_{BPT}[^{Et}\text{HPTA-O}^-][\text{BH}^+]$$

$$\frac{d[\text{BH}^+]}{dt} = -k_{BPT}[^{Et}\text{HPTA-O}^-][\text{BH}^+]$$

MATLAB files used to make the simulated TA traces

File 1: pyranine_kBPT.m, defines the differential equations for ^{Et}HPTA-O$^-$ and conjugate acid concentrations.

```
function [yprime] = pyranine_kBPT(t,y,k)
%differential equations for each species.
%1 = EtHPTAO-
yprime(1) = -(k(1).*y(1).*y(2));
%2 = conjugate acid
yprime(2) = -(k(1).*y(1).*y(2));

yprime = yprime(:);
end
```

File 2: example script used to set the input parameters and plot the data.

```
k = [1.93e10]; %rate constant of k_BPT
logtimespan = -6:0.2:-3; %from 1e-6 to 1e-3 in 0.2 increments logarithmically
timespanfast = 10.^logtimespan;
t0_conc = 8.9849e-08; %found from ΔOD measurements
abs_conc = 4.60185e-07; %found from absorbance measurements before laser
irradiation
%concentrations of [EtHPTAO-and [conjugate acid] respectively:
y0 = [(t0_conc + abs_conc),t0_conc];

[Tcalc,Ycalc]=ode23s(@(t,y)pyranine_kBPT(t,y,k),timespanfast,y0);
epsEtHPTAO = 75500; %extinction coefficient of EtHPTAO-
dOD_calc_548=((Ycalc(:,1) - abs_conc)*epsEtHPTAO);
semilogx(TA_548_t,pyridine_c1mM_548_dOD); %plots experimental data
hold on;
semilogx(Tcalc,dOD_calc_548,'ko'); %plots overlay of calculated data
hold off;
```

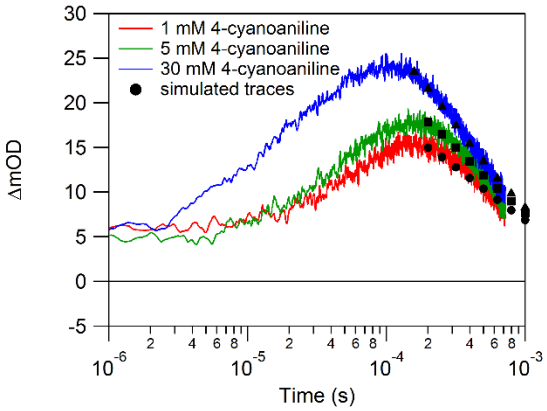

Figure S25. TA traces at 548 nm probing the decay of ^{Et}HPTA-O$^-$ through recombination with the conjugate acid, 4-cyanoanilinium. Simulated traces have been generated using the kinetics model (above) which are overlaid, showing good agreement with the experimental data.

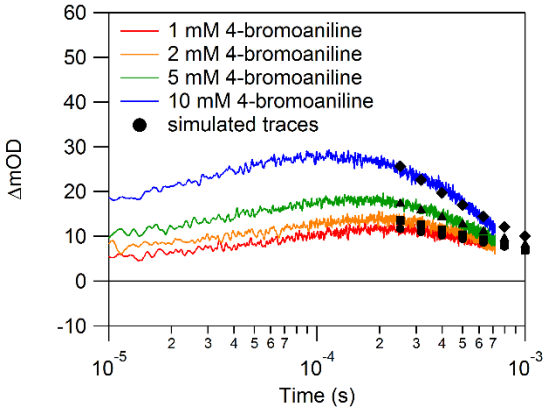

Figure S26. TA traces at 548 nm probing the decay of ^{Et}HPTA-O$^-$ through recombination with the conjugate acid, 4-bromoanilinium. Simulated traces have been generated using the kinetics model (above) which are overlaid, showing good agreement with the experimental data.

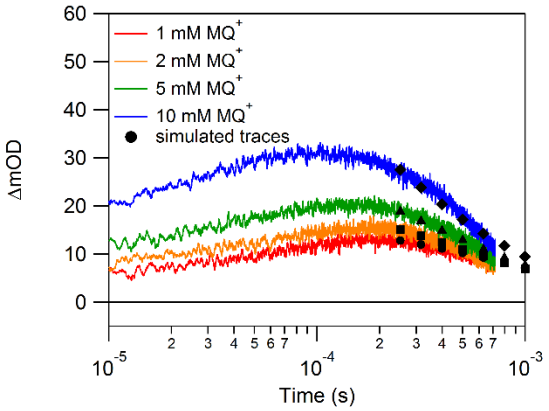

Figure S27. TA traces at 548 nm probing the decay of ^{Et}HPTA-O$^-$ through recombination with the conjugate acid, HMQ^{2+}. Simulated traces have been generated using the kinetics model (above) which are overlaid, showing good agreement with the experimental data.

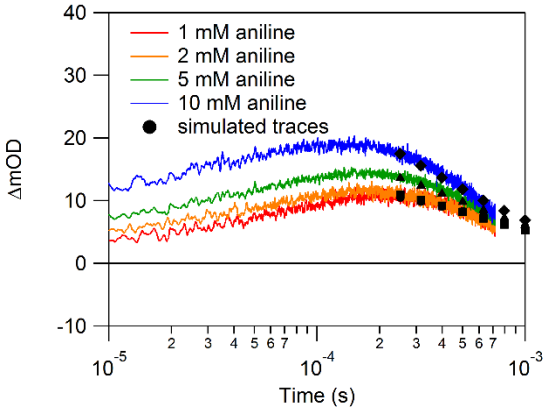

Figure S28. TA traces at 548 nm probing the decay of ^{Et}HPTA-O$^-$ through recombination with the conjugate acid, anilinium. Simulated traces have been generated using the kinetics model (above) which are overlaid, showing good agreement with the experimental data.

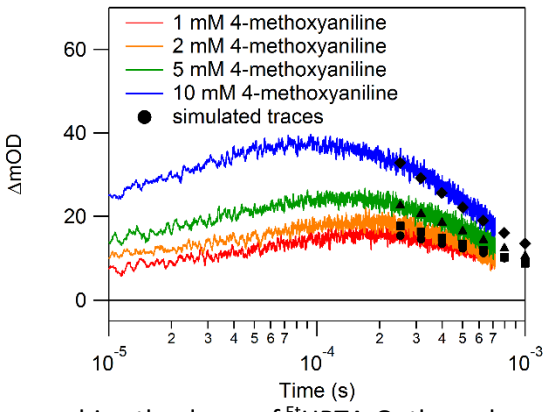

Figure S29. TA traces at 548 nm probing the decay of ^{Et}HPTA-O$^-$ through recombination with the conjugate acid, 4-methoxyanilinium. Simulated traces have been generated using the kinetics model (above) which are overlaid, showing good agreement with the experimental data.

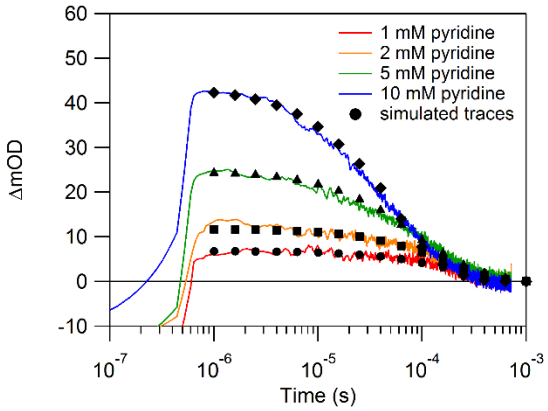

Figure S30. TA traces at 548 nm probing the decay of ^{Et}HPTA-O$^-$ through recombination with the conjugate acid, pyridinium. Simulated traces have been generated using the kinetics model (above) which are overlaid, showing good agreement with the experimental data.

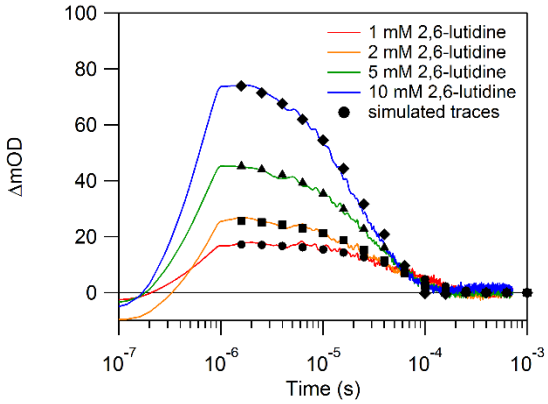

Figure S31. TA traces at 548 nm probing the decay of ^{Et}HPTA-O$^-$ through recombination with the conjugate acid, 2,6-lutidinium. Simulated traces have been generated using the kinetics model (above) which are overlaid, showing good agreement with the experimental data.

Table S1. Rate constants for the growth of the transient at 548 nm, obtained through fitting of the growth kinetics, and for back proton transfer, as estimated through kinetics modeling of the recombination of ^{Et}HPTA-O$^-$ with the conjugate acid.

Base:	4-cyano-aniline	4-bromo-aniline	MQ$^+$	aniline	4-methoxy-aniline	pyridine	lutidine
pK_a (BH$^+$)	7.0	9.43	10.4	10.62	11.86	12.56	14.14
$k_{g,obs}$ (M^{-1} s^{-1})	1.228 ± 0.061 × 10^6	2.098 ± 0.120 × 10^6	1.543 ± 0.002 × 10^6	1.692 ± 0.101 × 10^6	2.920 ± 0.142 × 10^6	-	-
k_{BPT} (M^{-1} s^{-1})	7.0×10^9	6.0×10^9	7.0×10^9	7.1×10^9	4.7×10^9	1.9×10^{10}	9.0×10^9

Characterization of ^{Et}HPTA-OH:

Figure S32. Full scan of ESI-MS of ^{Et}HPTA-O^{-} observed m/z = 622.17228, expected m/z = 622.17.

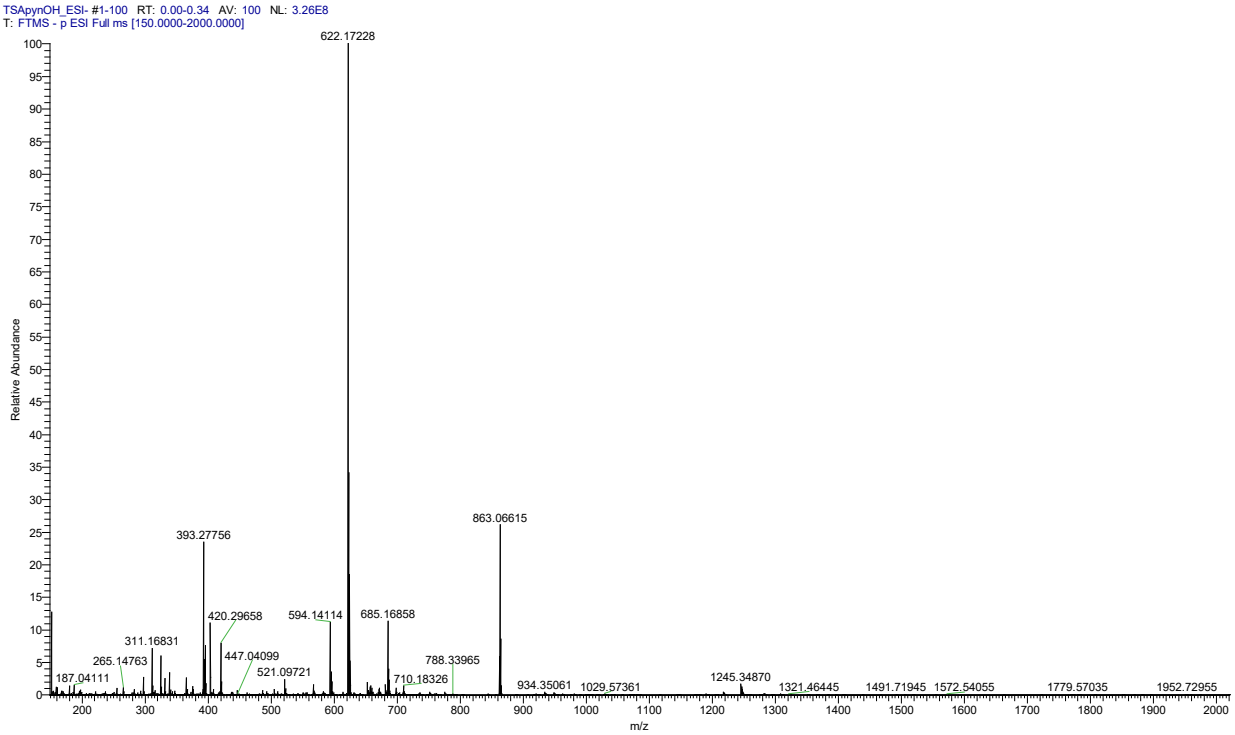

Figure S33. Zoom-in of peak at m/z = 622

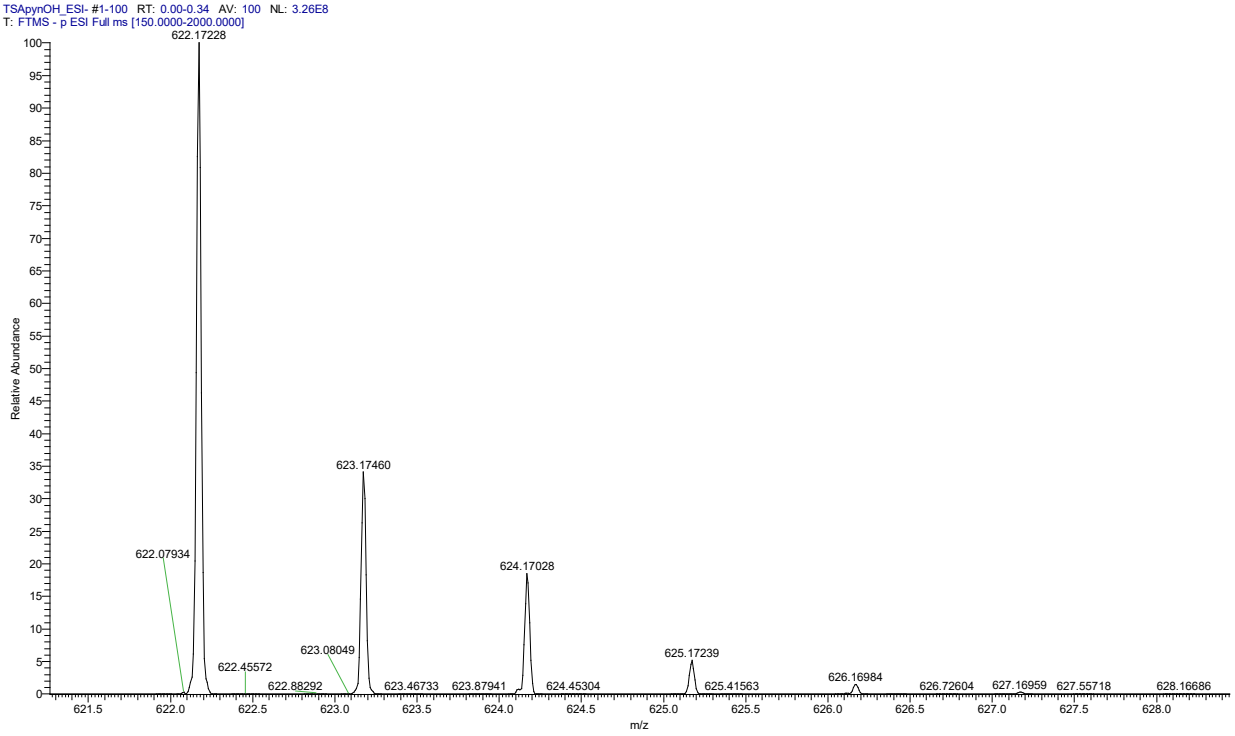

Figure S34. ^{1}H NMR spectrum of ^{Et}HPTA-OH ($CDCl_3$, 400 MHz). Minor ethyl acetate solvent impurities persist at 1.26 (t), 2.05 (s), and 4.08 (q) ppm. Inset shows zoom-in of aromatic region.

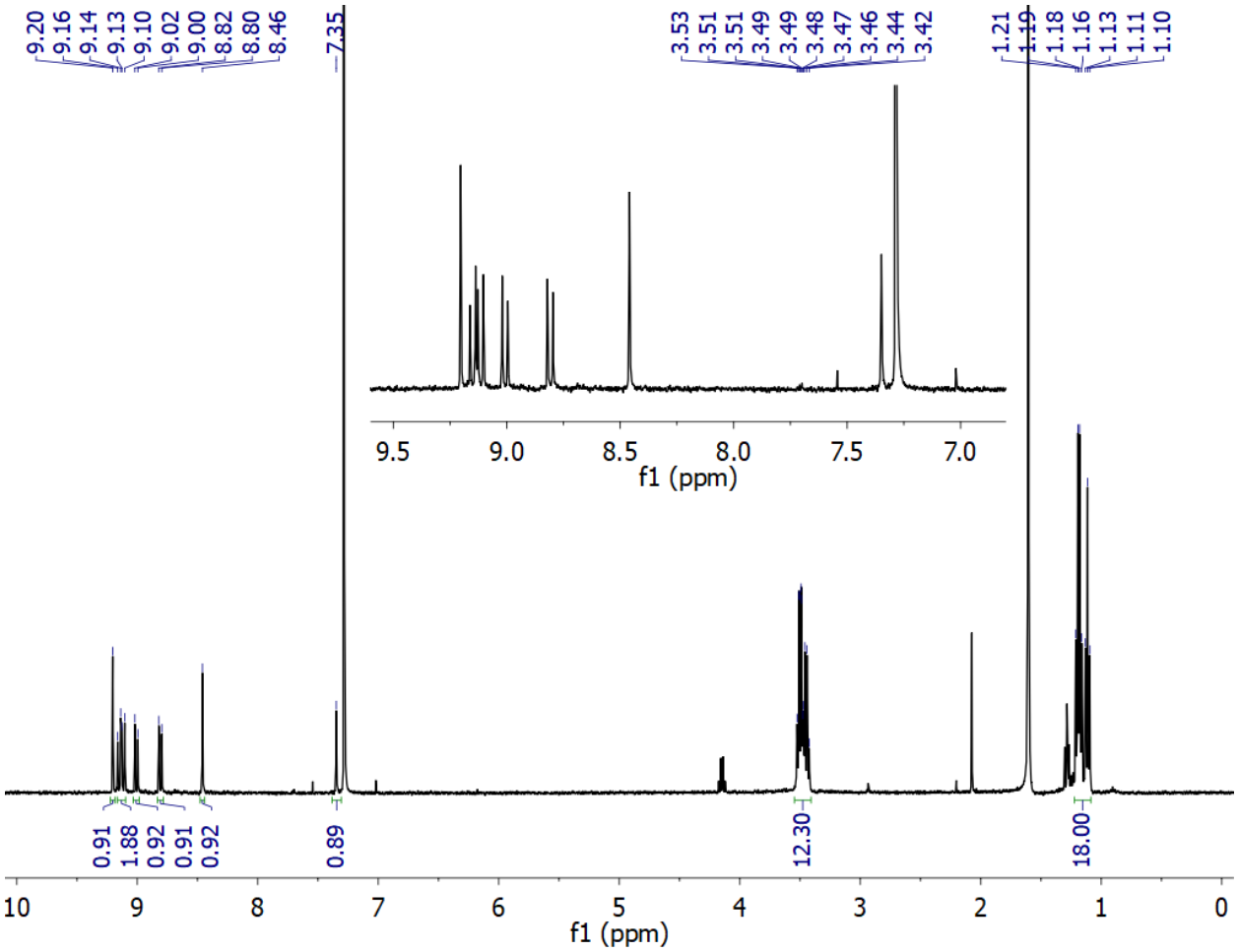

Figure S35. $^{13}C\{^{1}H\}$ NMR spectrum of ^{Et}HPTA-OH ($CDCl_3$, 400 MHz). Minor H grease impurity persists at 29.7 ppm. Insets show the asymmetric peaks of the ethyl groups.

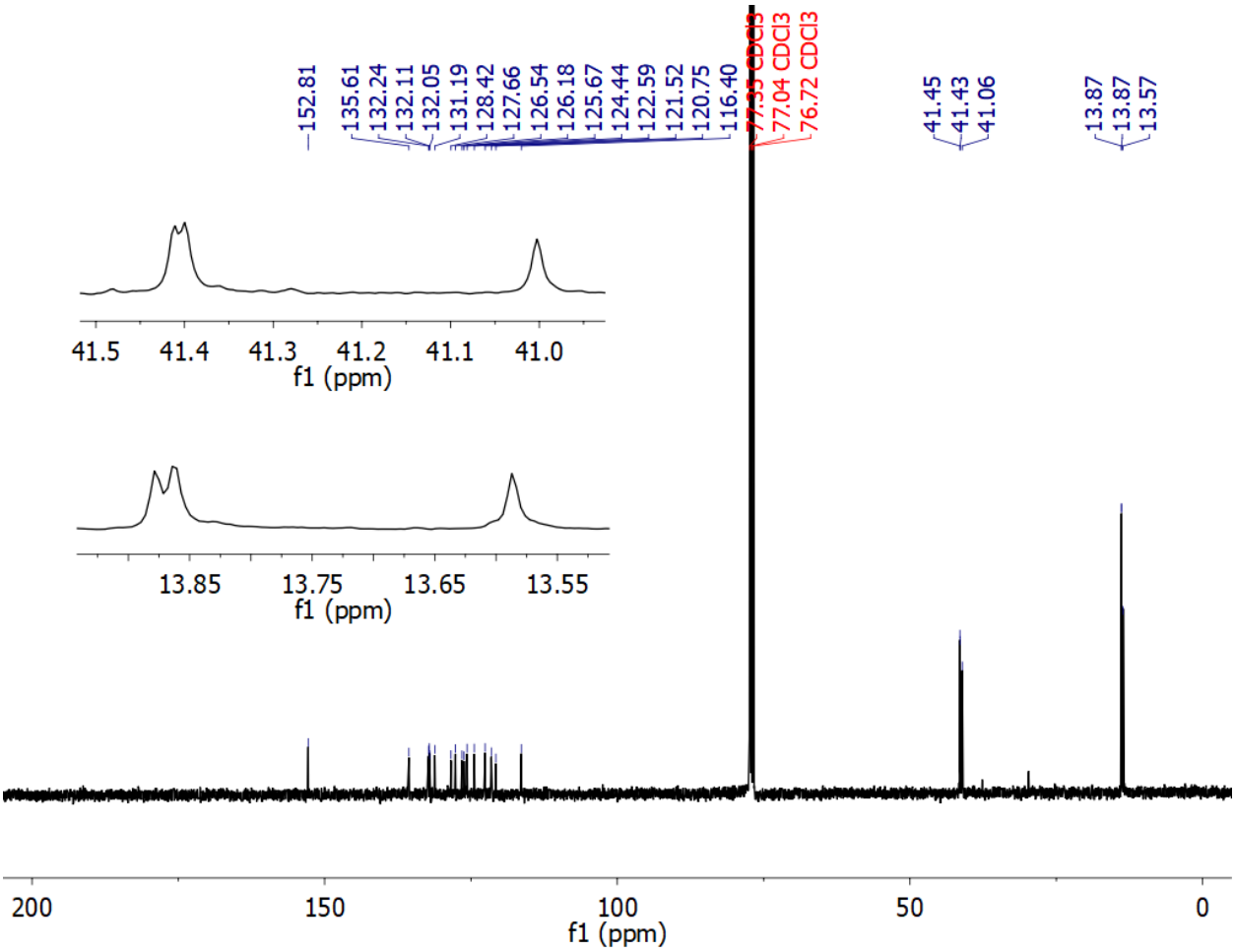

References:

(1) Finkler, B.; Spies, C.; Vester, M.; Walte, F.; Omlor, K.; Riemann, I.; Zimmer, M.; Stracke, F.; Gerhards, M.; Jung, G. Highly Photostable "super"-Photoacids for Ultrasensitive Fluorescence Spectroscopy. *Photochem. Photobiol. Sci.* **2014**, *13* (3), 548–562.

(2) Feng, D.-J.; Li, X.-Q.; Wang, X.-Z.; Jiang, X.-K.; Li, Z.-T. Highly Stable pseudo[2]rotaxanes Co-Driven by Crown Ether–ammonium and Donor–acceptor Interactions. *Tetrahedron* **2004**, *60* (29), 6137–6144.

(3) Spry, D. B.; Fayer, M. D. Observation of Slow Charge Redistribution Preceding Excited-State Proton Transfer. *J. Chem. Phys.* **2007**, *127* (20), 204501.

(4) Tran-Thi, T.-H.; Prayer, C.; Millié, P.; Uznanski, P.; Hynes, J. T. Substituent and Solvent Effects on the Nature of the Transitions of Pyrenol and Pyranine. Identification of an Intermediate in the Excited-State Proton-Transfer Reaction. *J. Phys. Chem. A* **2002**, *106* (10), 2244–2255.